Stanford Exploration Project, Report 120, May 3, 2005, pages 299–311

Orthogonal mesh generation for Riemannian wavefield extrapolation

Jeff Shragge[1]

ABSTRACT

This paper presents a general method for generating 2D or 3D orthogonal coordinate systems. Developed coordinate systems are triplication free and appropriate for use in Riemannian wavefield extrapolation. This method exploits properties of potential function solutions of Laplace's equation. I show that certain specifications of a potential function's boundary conditions lead to a physical representation of equipotential surfaces where there are equivalent to extrapolation steps. Potential function solutions, obtained through conjugate gradient solvers, are used subsequently in a phase-ray-tracing procedure that generates geometric rays orthogonal to the equipotential surfaces. These rays collectively define an orthogonal coordinate system linked to the underlying Cartesian mesh through definable one-to-one mappings. The utility of this approach in generating coordinate systems is tested on a 2D model of rugged topography from the Canadian Foothills, and on 3D topography of the San Francisco Bay area.

INTRODUCTION

Wave-equation imaging is computed almost exclusively on Cartesian meshes both for computational simplicity and because imaged subsurface volumes are usually rectangular parallelepipeds. However, situations exist where performing wave-equation imaging on more generalized coordinate system meshes is warranted. For example, extrapolating wavefields directly from an undulating topographic surface (Shragge and Sava, 2004a), orienting the extrapolation axis of lower-order operators in the direction of wavefield propagation to improve higher angle accuracy (Sava and Fomel, 2004), or imaging with overturning waves not currently modeled by one-way extrapolation operators (Shan and Biondi, 2004). Employing non-Cartesian meshes, though, necessitates resolving these three issues: which coordinate system should be chosen? how is the preferred coordinate system generated? and what are the appropriate governing wavefield extrapolation equations for this coordinate system choice?

Non-Cartesian wavefield extrapolation theory has advanced in recent years in the context of both global and exploration seismology. All of these methods locally transform the coordinate system and the corresponding governing propagation equations to a more appro-

[1]**email:** jeff@sep.stanford.edu

priate reference frame linked to an underlying Cartesian grid through one-to-one mappings. For example, Bostock et al. (1993) formulate an orthogonal, 2-D, plane-wave-centric coordinate system appropriate for propagating overturning teleseismic wavefields. Etgen (2002) and Shan and Biondi (2004) discuss the use of tilted coordinate systems that enable propagation of overturning waves with one-way extrapolation operators. Brandsberg-Dahl and Etgen (2003) and Sava and Fomel (2004) present generalized curvilinear coordinate and Riemannian metric formulations of the governing wavefield propagation equations, respectively.

Emerging with these developments are two classes of coordinate systems: those conformal with the propagating wavefield direction, and those conformal with pre-existing topology. Examples of the former include coordinate systems constructed by plane-wave decomposition (Bostock et al., 1993), and those generated using Eikonal equation ray-tracing (Sava and Fomel, 2004), whereas examples of the latter include a conformal mapping transform to incorporate surface topography (Shragge and Sava, 2004a). These methods, though, neither are universally applicable, nor always practical for 3D wavefield extrapolation. For example, ray-based methods can generate semi-orthogonal, triplicating coordinate systems that lead to numerical instability when propagating wavefields through coordinate system caustics. Another example is that the complex mathematics of conformal mapping surface topography does not extend easily to 3D. Hence, formulating a general approach for constructing 3D orthogonal coordinate systems appropriate for non-Cartesian wavefield extrapolation remains an open research topic.

This paper examines how potential function (PF) solutions of Laplace's equation, coupled with phase-ray tracing (Shragge and Sava, 2004b), can be used to generate orthogonal coordinate system meshes. Starting with appropriate PF boundary conditions, I generate a solution to Laplace's equation for any simply connected domain using conjugate gradient solvers (Claerbout, 1999). Importantly, the PF equipotentials define surfaces equivalent to wavefield extrapolation steps. The PF gradient field, by definition orthogonal to equipotentials, similarly forms geometric rays originating from the acquisition surface that collective form a ray coordinate system. The most obvious example is the Cartesian coordinate system, where each depth step surface represents an equipotential surface, and each vertical line projecting downward defines a coordinate system ray. Mathematical properties of a PF also guarantee that the 3D orthogonality of equipotential coordinate systems. Hence, this approach constructs computational meshes conformal to 3D geometric boundaries, including undulating 2D topographic surfaces or deviated wells found in vertical seismic profiling.

I begin this paper by reviewing some important properties of PF solutions of Laplace's equation, and then outline an approach for defining a Laplace's equation appropriate for incorporating generalized topology of a solution domain. Subsequently, I show how modified phase-ray tracing generates a suite of geometric rays that collectively form a coordinate system mesh. I then demonstrate the utility of the approach by developing a 2D coordinate system for the Canadian Rocky Mountain Foothills model discussed in Shragge and Sava (2004a) and a 3D coordinate system conformal to the 2D topography of the San Francisco Bay area.

THEORY

This section discusses some important characteristics of PF solutions of Laplace's equation (Kellogg, 1953), and outlines how these properties can be exploited to generate orthogonal coordinate systems. Using the scenario of 2D wave-equation migration from topography, I present appropriate boundary conditions, detail a method for obtaining potential function solutions, and outline a ray-tracing approach. These three components collectively define and algorithm for computing a geometric coordinate system.

Laplace's Equation

The scalar form of Laplace's equation is the partial differential equation,

$$\nabla^2\phi = 0 \tag{1}$$

where ∇^2 is the second-order spatial derivative operator, and ϕ is the sought PF. Laplace's equation is a special case of the Helmholtz differential equation,

$$\nabla^2\phi + k^2\phi = 0, \tag{2}$$

when wavenumber $k = 0$. A physical interpretation of this observation is that PF ϕ is the zero-frequency solution of the frequency-domain wave-equation, and is independent of the velocity field and thereby solely a geometric construct. A harmonic PF satisfying Laplace's equation has a number of important properties that are valid either on the boundary of, or entirely within, the defining domain. Most relevant to this discussion are that a PF:

- is uniquely determined by either the values, or normal derivatives thereof, on the domain boundary;
- has an average value over a spherical neighborhood equal to the value at its center; hence, PFs do not have local maxima or minima in the domain;
- is curl-free (i.e., $\nabla \times \phi = 0$) ensuring non-overlapping, and at most simply connected, equipotential surfaces;
- gradient field is uniquely defined, locally orthogonal to the equipotential surfaces, and related to the PF through,

$$\phi(b) - \phi(a) = \int_a^b \mathrm{d}\phi = \int_a^b \left(\frac{\partial\phi}{\partial x}\mathrm{d}x + \frac{\partial\phi}{\partial y}\mathrm{d}y + \frac{\partial\phi}{\partial z}\mathrm{d}z \right). \tag{3}$$

Each of these properties make PF solutions of Laplace's equation an important tool for generating orthogonal coordinate systems.

Generating Potential Functions

Generating orthogonal coordinate system meshes from PFs requires ascribing a physical interpretation to equipotentials: they are equivalent to extrapolation steps. Similarly, the characteristics of the PF gradient field are intrinsically related to geometric coordinate system rays. Figure 1 illustrates these concepts for the example of 2D wave-equation migration from topography. This scenario requires extrapolating a wavefield comprised of M traces into the subsurface a total of N steps, which ideally occurs directly from the topographic surface. The upper boundary of the computational domain, denoted $\tau_0(z,x)$ in this figure, is the acquisition surface. The lower boundary, denoted $\tau_N(z,x)$, is the desired flat subsurface datum. These two bounding surfaces are connected by two curves, $\gamma_1(z,x)$ and $\gamma_M(z,x)$, extending between the first and last extrapolation levels.

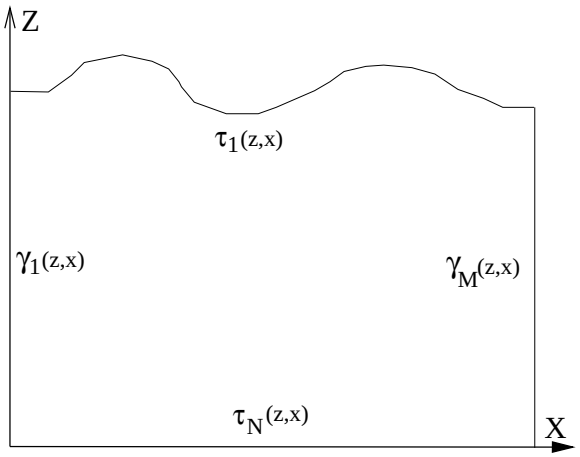

Figure 1: Scenario of migration from topography. The upper and lower topographic surfaces are denoted $\tau_0(z,x)$ and $\tau_N(z,x)$, respectively. Connecting vertical lines are denoted $\gamma_1(z,x)$ (left) and $\gamma_M(z,x)$ (right). The upper and lower surfaces have equipotential values of $\phi(\tau_0)=1$ and $\phi(\tau_N)=0$, respectively, whereas both side boundaries have zero normal derivatives. jeff1-topocoord [NR]

Solving for a PF satisfying Laplace's equation first requires specifying appropriate boundary conditions. Because distinct upper and lower equipotentials are desired, these two surfaces must have different constant values. Thus, I choose the following boundary conditions,

$$\phi(\tau_0)=1, \quad \phi(\tau_N)=0, \quad \left.\frac{\partial\phi}{\partial\mathbf{n}}\right|_{\gamma_1}=0, \quad \left.\frac{\partial\phi}{\partial\mathbf{n}}\right|_{\gamma_M}=0, \tag{4}$$

where the derivative with respect to variable $\mathbf{n}$ is in the direction outward normal to the surface represented by γ_1 and γ_M.

The Laplace's equation defined by the boundary conditions in Equation (4) is representable by a system of equations similar those commonly solved with conjugate gradient methods (Claerbout, 1999),

$$\mathbf{WLm} \approx 0 \tag{5}$$

subject to the following constraints,

$$(\mathbf{I}-\mathbf{W})(\mathbf{m}-\mathbf{m}_{bnd})=0, \tag{6}$$

where model vector **m** is the sought PF solution, $\mathbf{m}_{bnd}$ are the values on, and exterior to, the domain boundary, , $\mathbf{L} = \nabla^2$ is a Laplacian operator matrix, **W** is a mask operator indicating location of the boundary, and **I** is the identity operator.

I use the following algorithm to obtain PF solution, **m**:

1. Map the irregular topographic domain to a Cartesian mesh to generate vector $\mathbf{m}_{bnd}$;
2. Fix the PF values on the boundary of, and external to, the mapped domain using the mask operator **W**;
3. Initialize the model vector with a starting guess (i.e., $\mathbf{m}_0$) exploiting the smooth variation of ϕ between the upper and lower surfaces (i.e., through linear interpolation of ϕ on [1,0] between $\tau_0(z_0, x_0)$ and $\tau_N(z_1, x_0)$);
4. Solve system of equations in Equation (5) using a conjugate gradient algorithm (Claerbout, 1999), by allowing the solver to iterate until convergence is reached.

The resulting model vector, **m**, is the desired potential function that can be input to the phase ray-tracing algorithm described below. Finally, as illustrated by the example below, this approach is directly applicable to 3D computational domains because conjugate gradient solvers still work in 3D after the geometry is unwrapped on to a helical coordinate system (Claerbout, 1999).

Potential function ray tracing

The next processing step involves tracing geometric coordinate system rays from the generated PF. The goal here is to develop an orthogonal, ray-based coordinate system related to an underlying Cartesian mesh through one-to-one mappings,

$$\begin{aligned} \tau &= \tau(z,x,y) \\ \gamma &= \gamma(z,x,y) \qquad \text{where} \quad J = \frac{\partial(\tau,\gamma,\eta)}{\partial(z,x,y)} \neq 0, \\ \eta &= \eta(z,x,y) \end{aligned} \tag{7}$$

where τ is the wavefield extrapolation direction (equivalent to z in Cartesian), γ and η are the two orthogonal directions (equivalent to x and y in Cartesian), and J is the Jacobian of the coordinate system transformation. Recorded wavefield, $U(\tau_0, \gamma, \eta)$, is extrapolated from the acquisition surface defined by τ_0 into the subsurface along the rays coordinate system defined by triplet $\left[\tau, \gamma, \eta\right]$.

Geometric rays are traced by solving a first-order ordinary differential equation through integrating the PF gradient field along the gradient direction,

$$\delta\phi = \int_{a(z_0,x_0,y_0)}^{b(z_1,x_1,y_1)} ||\nabla\phi||^{-1} \left[\mathrm{d}z \frac{\partial\phi}{\partial z} + \mathrm{d}x \frac{\partial\phi}{\partial x} + \mathrm{d}y \frac{\partial\phi}{\partial y} \right], \tag{8}$$

where $a(z_0, x_0, y_0)$ is a known lower integration bound at equipotential $\phi(a)$, and $b(z_1, x_1, y_1)$ is an unknown upper integration bound located on equipotential surface, $\phi(b)$, and $||\nabla\phi||$ is the L^2 norm of the gradient function. The only unknown parameter is $b(z_1, x_1, y_1)$; hence, Equation (8) is an integral equation with an unknown integration bound. This approach is similar to phase-ray tracing method described in Shragge and Sava (2004b); however, in this case the integration step lengths are now unknown. Note also that the equipotentials of the upper and lower bounding surfaces in Equation (4) require PF steps of $\delta\phi = 1/N$.

The following approach locates unknown integration bound, b, on the next equipotential:

1. Numerically integrate Equation (8) on the interval $[a, a+\delta a]$ where δa is smaller than the expected step size, and test to see whether $\phi(a) - \phi(a+\delta a) > \delta\phi$; if yes goto step 3;
2. Numerically integrate Equation (8) on next interval $[a+\delta a, a+2\delta a]$ and test whether $\phi(a) - \phi(a+2\delta a) > \delta\phi$; if yes goto step 3; if no, repeat step 2 n times until true;
3. Linearly interpolate between points $a+(n-1)\delta a$ and $a+\delta a$ to find the b corresponding to $\phi(b) = \phi(a) - \delta\phi$.

A geometric ray is initiated at a particular $[\gamma_0, \eta_0]$ on acquisition surface defined by τ_0, and computed by integrating through each successive $\delta\phi$ step until the lower bounding surface τ_N is reached. This procedure is repeated for all γ and η acquisition points.

NUMERICAL EXAMPLES

2D Example - Canadian Foothills

The first test of the approach is on a 2D synthetic model characterized by rugged topography. This model is a merger of common geologic features from the Canadian Foothills in northeastern British Columbia, Canada (Gray and Marfurt, 1995). The velocity model, shown in Figure 2, consists of steep thrust fault planes and complex folds typical of a mountainous thrust region. The topographic boundary of interest is demarcated by the velocity model

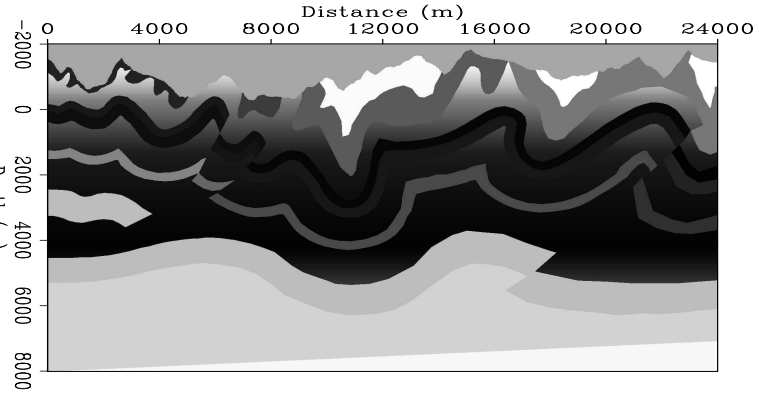

Figure 2: Example of 2D topography from the Canadian Foothills. Topographic surface is the first break in gray tone from the surface. jeff1-Foothills.vel [ER]

discontinuity nearest to the surface. The total relief of the model's surface is approximately 1600 m.

Figure 3 shows the test results. The flat datum surface is at a depth of 10000 m. Left-hand panels show the case where surface topography amplitudes are scaled down by 50%. The top left panel shows the 2-D potential function obtained through solution of Equation (5).

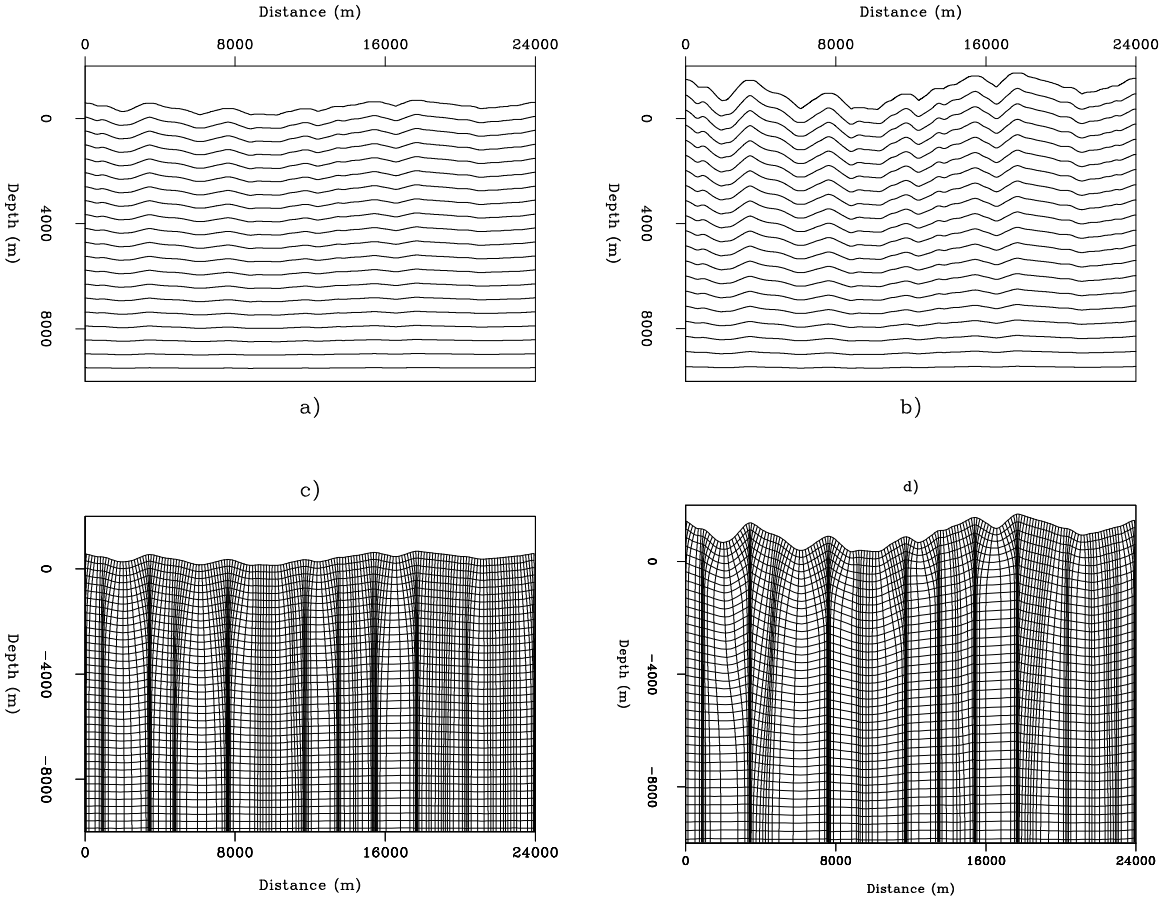

Figure 3: Potential functions and coordinate systems generated for the Canadian Foothills velocity model. a) Potential function with topography scaled down by 50%; b) Potential function with correct topography; c) coordinate system developed from the potential function of a); and d) coordinate system developed from the potential function of b). Note that increasing the amplitude of the topography tends to (de)focus the coordinate under topographic (lows) highs. jeff1-Plot2D [ER]

The PF is rougher nearer the surface, but smooths out to become uniform at the lower domain boundary. The bottom left panel shows the coordinate system ray-traced from the PF presented in the top left panel. Note that the coordinate system focuses beneath topographic maxima, and defocuses under topographic minima. This demands that the Jacobian value in Equation (7) diverge from unity.

The right-hand panels of Figure 3 show results similar to those in the left-hand panels, except that the true topographic surface is restored. The top right panel shows a rougher PF,

which is expected due to the increased topographic rugosity. The bottom right panel presents the coordinate system ray-traced from the PF shown in the upper right panel. Relative to that the bottom left panel, this coordinate system exhibits increased focusing and defocusing under topographic maxima and minima, respectively.

3D Example - San Francisco Bay area Topography

Using the elevation map of the San Francisco Bay area illustrated in Figure 4, a second test was conducted to assess the applicability of the method in 3D. The maximum surface topographic relief is approximately 800 m; however, the elevation gradients and topographic wavelengths are significantly smaller and longer than the 2D test illustrated in Figure 2. The flat subsurface datum is set a depth of 8000 m. Figure 5 presents the slices through the 3D potential function

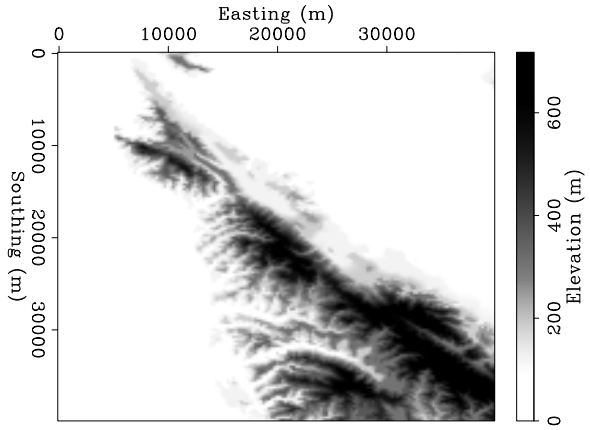

Figure 4: Elevation map of the San Francisco Bay area used in 3D testing. jeff1-Bay.2D [ER]

results. The top panel shows a depth slice at approximately zero elevation, whereas the lower two panels show slices along Easting (bottom left) and Southing (bottom right) directions. These profiles illustrate a PF that is smoother than the previous example.

Figure 6 shows the coordinate system generated along the same two slices shown in the panels b) and c) of Figure 5. The generated coordinate system much smoother than in the previous example, as expected from the smoothness of the PF. Figure 7 presents a perspective view of the ray-traced coordinate system results. The coordinate system rays are fairly straight, except in the region beneath topographic highs. Another way to visualize the ray coordinate system is to examine how the topography 'heals itself' at various τ steps. Figure 8 illustrates this for the τ_0 (top left), $\tau_{N/3}$ (top right), $\tau_{2N/3}$ (bottom left) and τ_N (bottom right) surfaces, where N is the total number of extrapolation steps. The sidebars show the elevation difference between the lowest and highest points of each equipotential surface. The greyscale intensity has been clipped according to the maximum elevation difference at τ_0.

DISCUSSION AND FUTURE WORK

These examples indicate that the procedure developed in this paper can generate coordinate systems from potential function solutions of Laplace's equation. Tests were conducted on

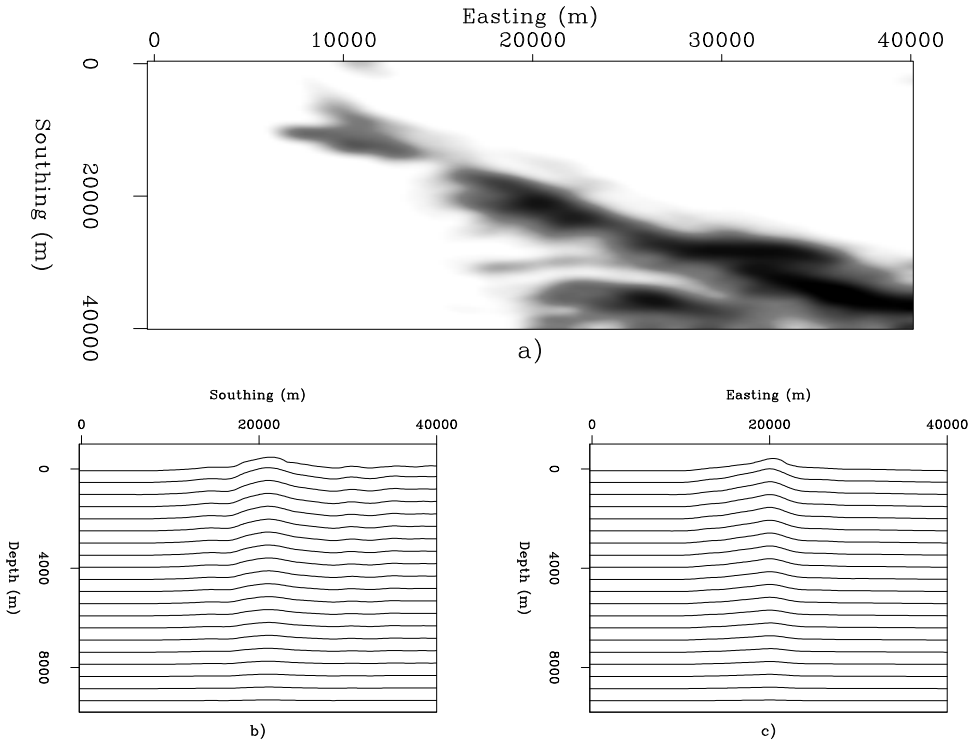

Figure 5: 3D potential function for San Francisco Bay area topography. a) depth slice of the potential function at approximately zero elevation; b) vertical slice along Southing 20 km; and c) vertical slice along Easting 20 km. Note that the potential function is smoother than the previous example indicating less coordinate system focusing. jeff1-Pot3D [ER]

surfaces exhibiting moderate-to-rough topography; hence, coordinate surfaces developed for smoother surfaces (e.g., deviated VSP wells) should be subject to less focusing than these examples. Thus, I assert that PF-derived smooth coordinate systems should be good for use in RWE.

However, as the 2D rugged topography example indicates, coordinate systems under rough topography generated by this approach probably are less well-suited for RWE. In particular, the 2D example probably reveals that coordinate system generated through the conformal mapping approach of Shragge and Sava (2004a) are probably better suited for RWE. This is because wavefield extrapolation on severely focused coordinate systems requires high extrapolation operator accuracy. However, the real test of whether coordinate systems generated by the above approach are appropriate for RWE ultimately lies in accurcy of resulting extrapolated wavefields and corresponding images.

CONCLUDING REMARKS

Generating 2D and 3D coordinate systems using geometric ray-tracing on potential function solutions of Laplace's equation is a viable approach. Because of certain properties of potential

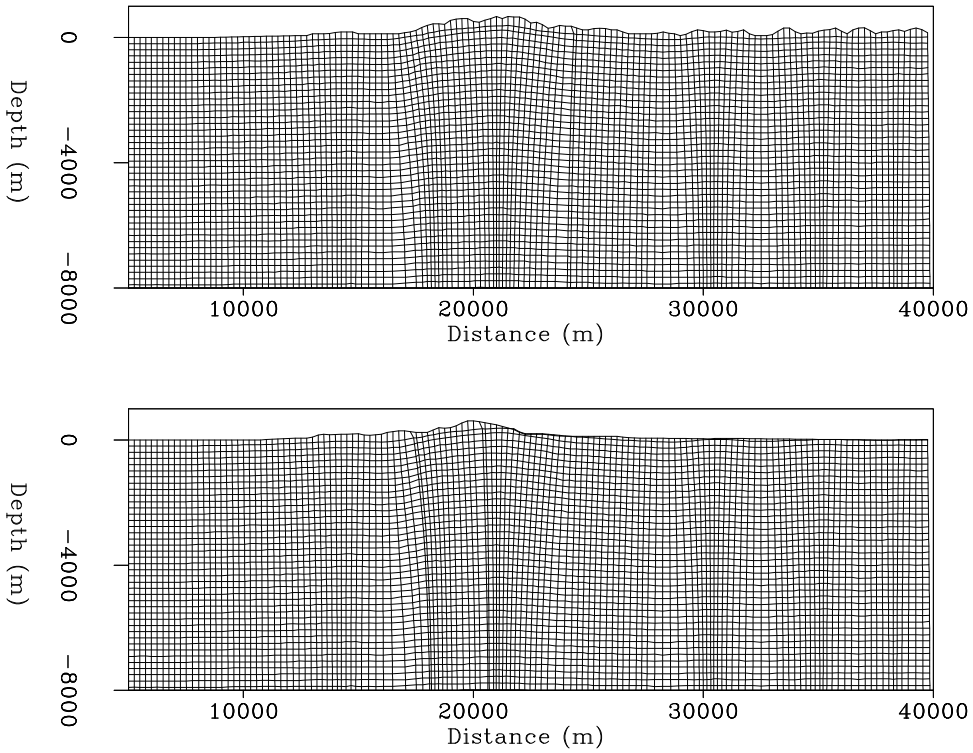

Figure 6: Cross-section of the 3-D coordinate system developed for the San Francisco Bay area topography. Left-hand panel: vertical slice along along Southing 20 km; and right-hand panel: vertical slice along Easting 20 km. jeff1-Ray.slice [ER]

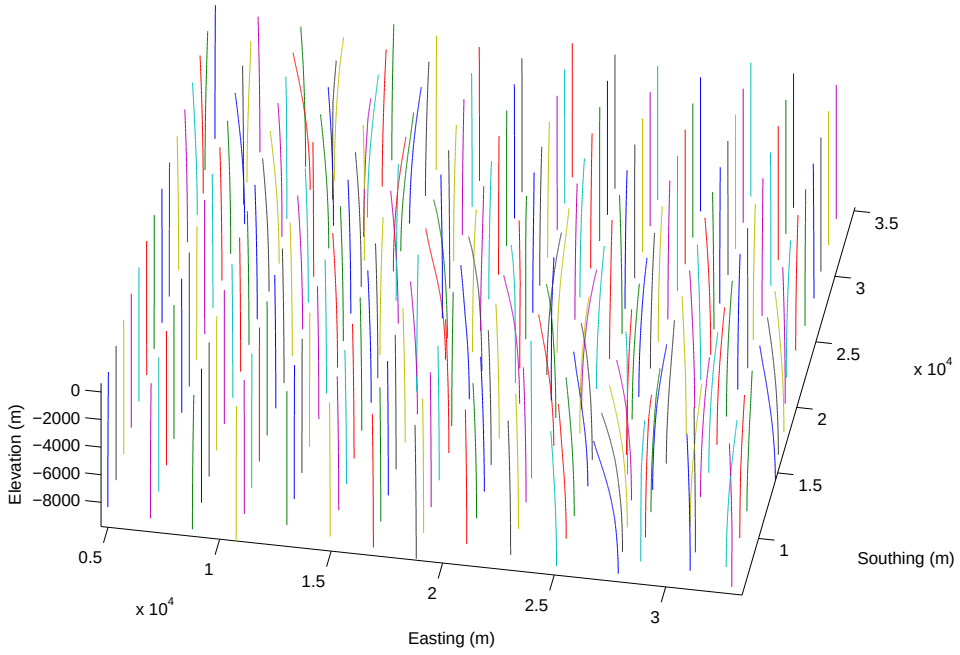

Figure 7: Perspective view of the ray-traced coordinate system developed from potential function in Figure 5. jeff1-Rays3D [CR]

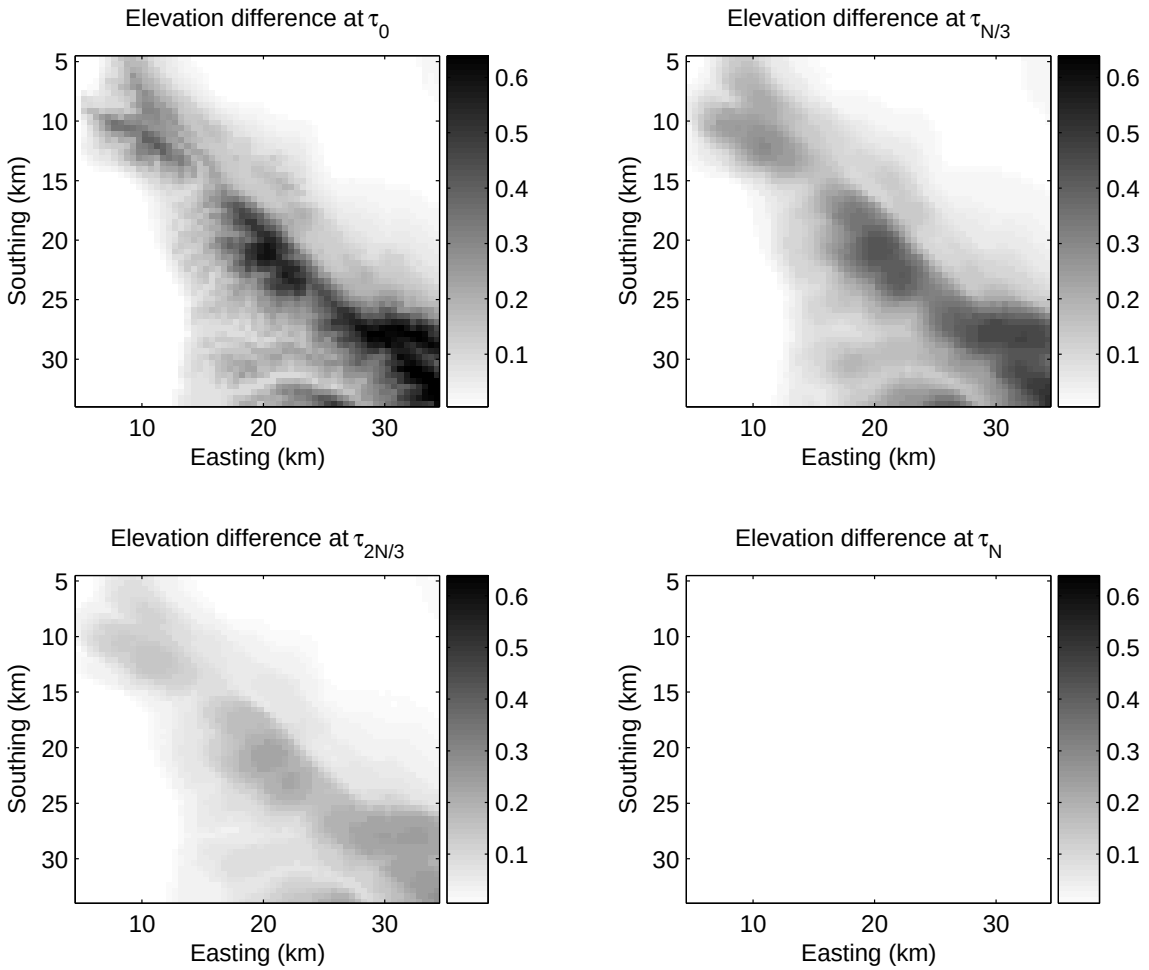

Figure 8: Illustration of topographic coordinate system healing through examination of single-extrapolation step elevation differences (in km). Top left: step τ_0; top right: step $\tau_{N/3}$; bottom left: step $\tau_{2N/3}$; and bottom right: step τ_N. Sidebar shows the elevation differences (in km), where the greyscale has clipped according to the peak elevation difference at τ_0. jeff1-Rays3D2 [CR]

functions, ray-traced coordinate systems are guaranteed to be orthogonal. Importantly, these coordinate systems are appropriate for 3D Riemannian wavefield extrapolation, and can be applied in numerous scenarios, including wave-equation migration directly from an undulating 2D topographic surface, and VSP imaging from deviated wells.

ACKNOWLEDGMENTS

Paul Sava assisted in the early development of the potential field approach. I would also like to thank Biondo Biondi and Brad Artman for helpful discussions.

REFERENCES

Bostock, M., VanDecar, J., and Snieder, R., 1993, Modeling teleseismic P-wave propagation in the upper mantle using a parabolic approximation: Bulletin of the Seismological Society of America, **83**, 756–779.

Brandsberg-Dahl, S., and Etgen, J., 2003, Beam-wave imaging: Soc. of Expl. Geophys., Expanded Abstracts, 977–980.

Claerbout, J., 1999, Geophysical estimation by example: Environmental soundings image enhancement: Stanford Exploration Project, `http://sepwww.stanford.edu/sep/prof/`.

Etgen, J., 2002, Waves, Beams and Dimensions: an illuminating if incoherent view of the future of migration: Soc. of Expl. Geophys., invited presentation.

Gray, S., and Marfurt, K., 1995, Migration from topography: Improving the near-surface image: J. Can. Soc. Expl. Geophys., **31**, 18–24.

Kellogg, O., 1953, Foundation of Potential Theory: Dover Publications, Inc., New York.

Sava, P., and Fomel, S., 2004, Seismic imaging using Riemannian wavefield extrapolation: Submitted to Geophysics.

Shan, G., and Biondi, B., 2004, Wavefield extrapolation in laterally-varying tilted TI media: SEP–**117**, 1–10.

Shragge, J., and Sava, P., 2004a, Incorporating topography into wave-equation imaging through conformal mapping: SEP–**117**, 27–42.

Shragge, J., and Sava, P., 2004b, Adaptive phase-ray wavefield extrapolation: SEP–**115**, 13–28.